Journal of Magnetism and Magnetic Materials 510 (2020) 166941

Contents lists available at ScienceDirect

Journal of Magnetism and Magnetic Materials

journal homepage: www.elsevier.com/locate/jmmm

Research articles

The effect of divalent ions of zinc and strontium substitution on the structural and magnetic properties on the cobalt site in cobalt ferrite

Parvin Imanipour[a], Saeed Hasani[a,*], Mohammad Afshari[a], Shiva Sheykh[a], Amir Seifoddini[a], Khadijeh Jahanbani-Ardakani[b]

[a] Department of Mining and Metallurgical Engineering, Yazd University, 89195-741 Yazd, Iran
[b] Department of Industrial Engineering, Meybod University, Meybod, Iran

ARTICLE INFO

Keywords:
Divalent ion
Nanocomposite
Rietveld refinement method
Magnetic properties

ABSTRACT

The effect of doping of divalent Sr^{2+} and Zn^{2+} ions on the structural and magnetic properties of cobalt ferrite was investigated. For this purpose, the samples with the composition of $Co_{1-x-y}Sr_xZn_yFe_2O_4$ (where x = 0.0, 0.01, 0.05, 0.3 and y = 0.0, 0.05, 0.1, 0.4, 0.5, 0.7) were synthesized by using the spontaneous gel auto-combustion (Pechini) technique. The effect of the presence of these dopants on the average of crystallite/grain size, lattice parameter, density, the purity of the formed phase, and morphology of the synthesized nanoparticles was determined. Although formation of spinel ferrite was confirmed in the all samples, the secondary phase of $SrFeO_{2.86}$ was detected for the samples containing high values of Sr (=0.3). Also, thermal DTA-TG analysis showed that the formation enthalpy of the doped-samples was increased. FE-SEM micrographs showed a semi-spherical morphology, regular and well-distributed nanoparticles in the samples with high values of these dopant elements. According to the FTIR data, simultaneous doping of Sr^{2+} and Zn^{2+} ions caused to a slightly shift in spectrum. The magnetic characterization of the synthesized samples revealed that the simultaneous doping of Sr^{2+} and Zn^{2+} ions in cobalt ferrite drastically changes the magnetic parameters of cobalt ferrite. For instance, the saturation magnetization and coercivity values were changed from 72 to 4 emu/g and from 1019 to 5 Oe, respectively. Furthermore, the hard magnetic behavior of cobalt ferrite changed to the superparamagnetic behavior in the doped-samples.

1. Introduction

Among all ferrites, researchers believe that spinel ferrites are a group of magnetic materials which have a large number of advantages for technological and scientific applications due to their excellent physical and chemical properties [1–5]. Spinel can be represented by the general formula MFe_2O_4 (M = Co, Ni, Zn, Mn, Cu, etc), in which the metal cations A and B are fitted at both A (tetrahedral) and B (octahedral) interstitial sites in the face centered cubic (FCC) formed by arrangement of oxygen anions [1,6–8]. Among the spinel ferrites, $CoFe_2O_4$ (CF) is known as a well-known partially ferromagnetic ferrite with unique properties such as the strong magneto-crystalline anisotropy, suitable chemical and thermal stability, high coercivity (H_c), high Curie temperature and moderate saturation magnetization (M_s) [9,10]. These excellent characteristics make CF as a candidate for nano-biotechnology, microwave absorbers, drug delivery systems with lower side effects, ferrofluids applications and developing of biosensors used for clinical and environmental purposes [9,11–14]. By the way, it is notable that the physical and chemical properties of these nanoparticles are dependent on several parameters such as preparation technique, pH, synthesis parameters (i.e. calcination time and temperature), presence of dopants and capping agents, distribution of metal cations, nature of initial materials and characteristics of final nanoparticles (i.e. size, morphology, etc.) [15–19]. For instance, there are several chemical, physical and mechanical methods to synthesis of ultra-fine cobalt such as sonochemical [20,21], hydrothermal [22,23], thermal decomposition [24,25], co-precipitation [26–28], and sol-gel [29–33] methods. Among these methods, the sol-gel auto-combustion method is known as one of the most sufficient methods duo to lower annealing temperature and time, more simple procedure and synthesis of nanomaterials with high purity and lower cost [9,13,34,35]. On the other hand, it is notable that the doping of alloying elements can affect by the fraction of Co^{2+} ions occupied in the octahedral sites and therefore leads to change the main properties of cobalt ferrite nanoparticles [36]. Hence, there are numerous scientific investigations, so that the effect of presence of doped elements such as Al [34], Ti [37], Cd [17], Ni

* Corresponding author.
E-mail address: hasani@yazd.ac.ir (S. Hasani).

https://doi.org/10.1016/j.jmmm.2020.166941
Received 17 January 2020; Received in revised form 29 February 2020; Accepted 22 April 2020
Available online 23 April 2020
0304-8853/ © 2020 Elsevier B.V. All rights reserved.

[11],Cu [12,38], Ag [4], In [6], V [39], Zn [12,17], Mn [12], Cr [40], and rare earth elements [40–42] on the CF properties has been investigated. Among these elements, zinc and strontium are introduced as two effective elements on the magnetic properties of CF. Based on the previous publications [17,43], substitution of zinc ions at the place of Co^{2+} ions into the cobalt ferrite decrease the size of CF nanoparticles and improves the chemical stability, corrosion resistivity, and magneto–crystalline anisotropy. Singh et al. [44] showed a transition from ferromagnetic to super-paramagnetic behavior with an increase in Zn ions content. In addition, other researchers showed that, magnetic properties of cobalt ferrite such as saturation magnetization (M_s), coercivity (H_c), Curie temperature (T_c), and anisotropy constant (K) decrease by increasing of Zn ions [45,46]. Also, strontium as a non-magnetic alkaline earth metal with a suitable atomic radius is an adequate candidate compared with other alkaline elements such as Co and Ba [19,47]. Kumar et al. [19] showed that M_s as well as H_c and particle size are reduced with an increase in the content of the doped Sr at the place of Co^{2+} ions into the cobalt ferrite, while residual strain in the crystal structure is increased due to an increase in the lattice parameter with an increase in the content of the doped Sr. Also, $SrCO_3$ and $SrFeO_{2.96}$ paramagnetic phases were formed in the presence of Sr ions because of low solubility of Sr in the CF structure [19]. Nevertheless, the effect of the simultaneous presence of Zn and Sr divalent ions on the structural and magnetic properties of CF nanoparticles has not been investigated yet. Hence, in the present study, CF magnetic nanoparticles were synthesized in the simultaneous presence of these two elements by the sol–gel auto-combustion technique.

2. Materials and experimental details

2.1. Materials

All media components used in this study, including Cobalt (II) nitrate hexahydrate ($Co(No_3)_2{\cdot}6H_2O$, ≥99%), iron (III) nitrate nonahydrate ($Fe(NO_3)_3{\cdot}9H_2O$, ≥99%), Strontium nitrate ($Sr(No_3)_2$), ≥99%), Zinc nitrate tetrahydrate ($Zn(NO_3)_2{\cdot}4H_2O$, ≥99%), citric acid ($C_6H_8O_7$, ≥99.5%), and ammonia (NH_3, ≥25%) were purchased from Merck (Darmstadt, Germany).

2.2. Synthesis of nanoferrites

Sol-gel method was employed to synthesis of nanoparticles with composition of $Co_{1-x-y}Sr_xZn_yFe_2O_4$, where chemical composition of these specimens is presented in Table 1. For this purpose, first, stoichiometric amounts of metal nitrates in the aqueous solution of citric acid were dissolved in minimum amount of double distilled water and were stirred by a magnetic stirrer at 300–400 rpm until a transparent solution was obtained. It is notable that the molar amount of citric acid was increased twice as much as nitrates. To stabilize the as-formed solution, pH value of the solution was adjusted to ~6 by the addition of ammonia. At the next stage, a dense gel was created by stirring the solution at 80 °C. In the following, the obtained gel was subjected to a self-propagating combustion process with an increase in temperature up to 300 °C and then the flaky loose CF powders were obtained. At the last stage, to obtain cubic structure of CF nanoparticles, the combusted powders were calcinated at 800 °C for 3 h in the air atmosphere.

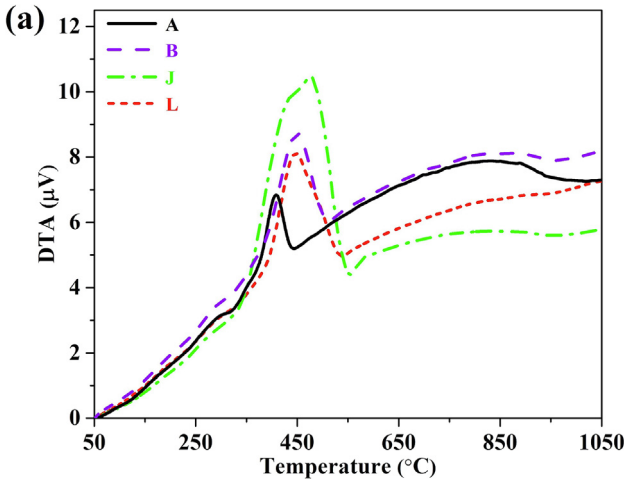

Fig. 1. (a) DTA and (b) TG curves related to the selected samples.

Fig. 1. (*continued*)

Table 1
Chemical composition and structural parameters of the synthesized samples.

Sample Code.	Chemical Composition	Crystallite size (nm)		Lattice parameter (Å)	Volume (Å^3)	X-ray density (g/cm^3)
		XRD	FE-SEM			
A	$CoFe_2O_4$	88.2	77.1	8.39275	591.17	5.27
B	$Co_{0.5}Zn_{0.5}Fe_2O_4$	31.1	52.1	8.38536	589.61	5.36
C	$Co_{0.89}Sr_{0.01}Zn_{0.1}Fe_2O_4$	27.2	44.6	8.38437	589.40	5.30
D	$Co_{0.59}Sr_{0.01}Zn_{0.4}Fe_2O_4$	30.4	–	8.42470	597.94	5.27
E	$Co_{0.29}Sr_{0.01}Zn_{0.7}Fe_2O_4$	30.6	–	8.42926	598.91	5.30
F	$Co_{0.9}Sr_{0.05}Zn_{0.05}Fe_2O_4$	21.4	40.6	8.38536	589.61	5.32
G	$Co_{0.85}Sr_{0.05}Zn_{0.1}Fe_2O_4$	23.9	–	8.39976	592.65	5.30
H	$Co_{0.55}Sr_{0.05}Zn_{0.4}Fe_2O_4$	20.5	–	8.42409	597.81	5.30
I	$Co_{0.25}Sr_{0.05}Zn_{0.7}Fe_2O_4$	23.0	–	8.43051	599.18	5.33
J	$Co_{0.6}Sr_{0.3}Zn_{0.1}Fe_2O_4$	19.8	30.7	8.39355	591.33	5.47
K	$Co_{0.3}Sr_{0.3}Zn_{0.4}Fe_2O_4$	15.6	–	8.42083	597.12	5.47
L	$Sr_{0.3}Zn_{0.7}Fe_2O_4$	18.2	29.1	8.43807	600.79	5.47

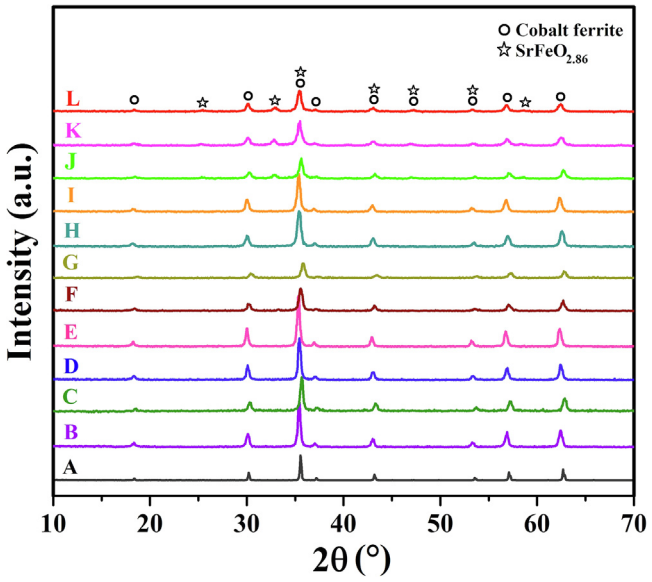

Fig. 2. XRD patterns of the synthesized samples.

2.3. Characterization of ferrite nanoparticles

To evaluate the phase analysis and structural characterizations of the synthesized $CoFe_2O_4$ nanoparticles, the X-ray diffraction method was employed by an XRD instrument (PW1730 PHILIPS, Netherland) using Cu kα radiation (λ = 0.1540 nm) with a working voltage and current of 40 kV and 30 mA, respectively. Also, the crystallite size and lattice parameter was refined by the Rietveld refinement method utilizing PANalytical X'Pert HighScore Plus software. In addition, to determine the effect of the presence of doping elements (strontium and zinc) on the temperature characteristics of the decomposition process and thermal behavior of the combusted powder during the calcination process, the flaky loose $CoFe_2O_4$ powders were subjected to DTA-TG thermal analysis (STA504, Bahr, USA) at a heating rate of 20 °C/min from ambient temperature up to 1200 °C in the air atmosphere. The Fourier transform infrared spectroscopy were carried out using FT-IR instrument (Avatar, Thermo, USA) in the wavenumber spectrum of 400–4000 cm^{-1}. Also, the effect of presence of the doping elements on the microstructure and particles size distribution of the synthesized nanoparticles was investigated by using FE-SEM (MIRA 3, TESEAN, Czech Republic). The magnetic properties were measured via VSM (Magnetic Daghigh Daneshpajouh, Iran) at room temperature up to a magnetic field of 1 T.

3. Results and discussion

3.1. DTA-TG analysis

Thermal analysis methods are used to study the mechanism and thermal behavior of the systems [48,49]. Fig. 1 illustrates thermal behavior and temperature characteristics of the decomposition procedure of the flaky loose powders for the samples A, B, J, and L. As seen in Fig. 1(a), there are two different stages within the DTA curves, so that for free-doped sample (sample A) there are two exothermic peaks in the temperature ranges of 325–450 °C and 450–925 °C, respectively. On the other hand, the first exothermic DTA peak is accompanied with a large weight loss in TG curves. Therefore, this stage is related to the auto-combustion process. The weight loss occurred at this stage is probably related to oxidative decomposition of organic compounds, which is in good agreement with that of reported by others [7,9,50–56]. As shown, sharper combustion peaks are observed for the samples doped by Zn and Sr (i.e. B, J and L) in comparison with the sample A. The enthalpy of formation of Co, Zn, and Sr ferrites are estimated to be −1087.8 [57], −1179.1 [58], and −1583.8 [59] kJ/mol. Therefore, this increase in the intensity of the first DTA peak can be due to an increase in the enthalpy of formation as a result of substitution Zn and Sr on the Co sites. Furthermore, size of the synthesized nanoparticles can be

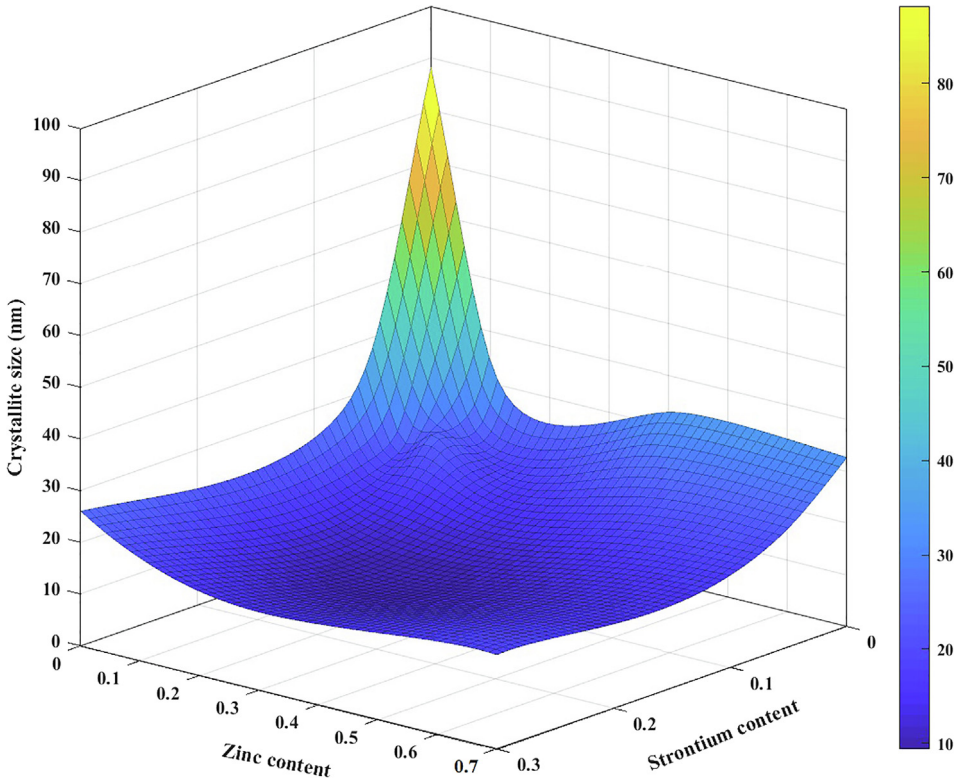

Fig. 3. Variation of the average of crystallite size as a function of Zn and Sr contents.

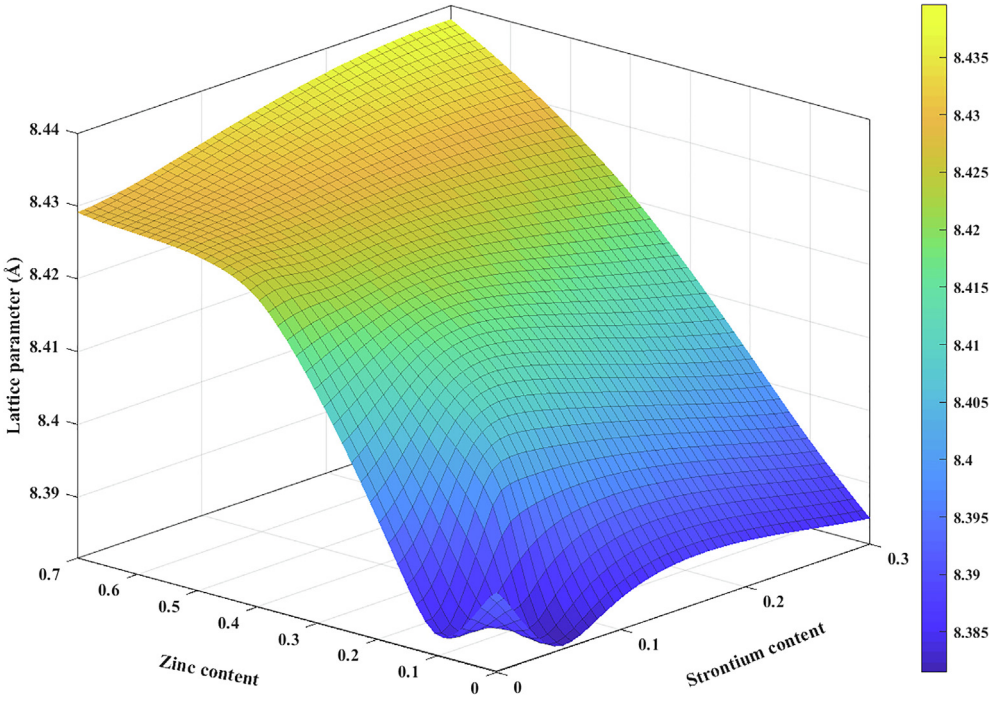

Fig. 4. Variation of lattice parameter as a function of Zn and Sr contents.

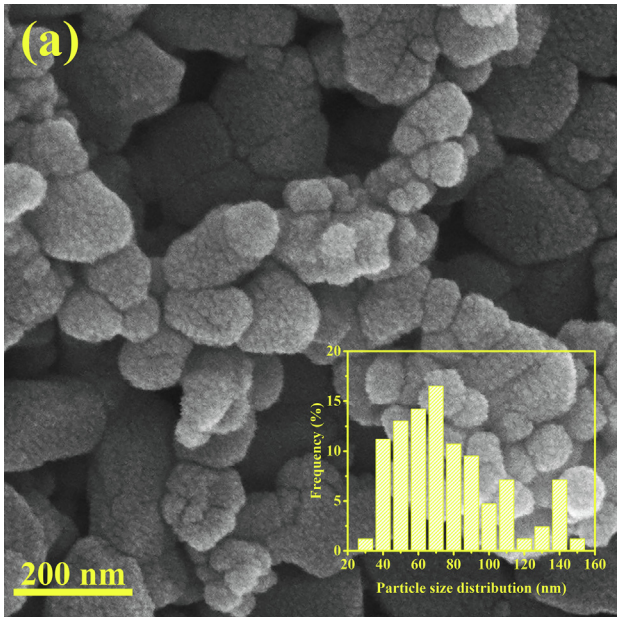

Fig. 5. FE-SEM micrographs of the synthesized samples (a) A, (b) B, (c) C, (d) F, (e) J, and (f) L.

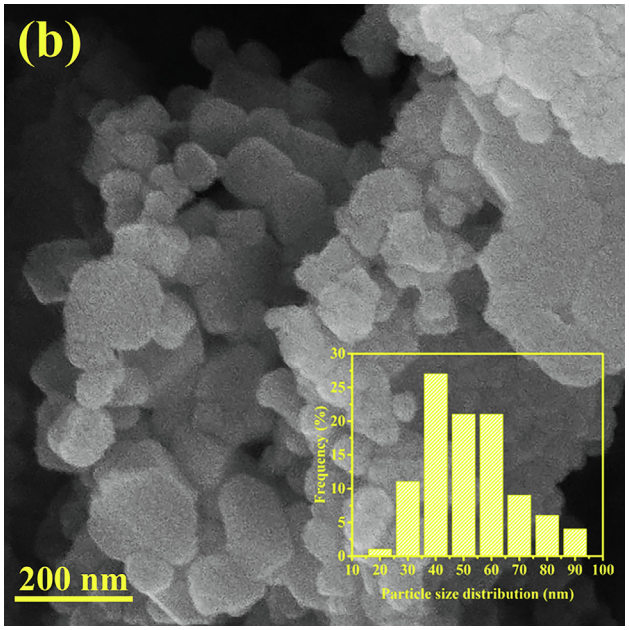

Fig. 5. (*continued*)

considered as another effective parameter on intensity of the DTA peak, because the smaller size of the nanoparticles, the higher surface of particles and the more surface energy [60]. However, similar results can be observed in other studies [56,61]. For instance, Hashemi et al. [61] showed that the intensity of the DTA peak is directly proportional to the total surface area of the synthesized particles.

On the other hand, the second exothermic DTA peak, as a broad exothermic peak, is attributed to the powder densification [55]. As shown, no weight loss is observed above 500 °C in the TG curves, meaning that pure cobalt ferrite nanoparticles can be formed above this temperature. Thus, in order to synthesis of Sr-Zn doped cobalt ferrite without any organic waste, the precursors were calcined at 800 °C for 3 h.

3.2. Phase analysis

Fig. 2 shows XRD patterns of the calcined samples with compositions of $Co_{1-x-y}Sr_xZn_yFe_2O_4$ (where; x = 0.0, 0.01, 0.05, 0.3 and y = 0.0, 0.05, 0.1, 0.4, 0.7). As seen, there are typical diffraction characteristic peaks of cubic spinel structures (JCPDS card No. 22–1086) for all samples, which is in good agreement with that reported by others [62–64]. Although, in most samples, no additional peaks are observed, but a secondary phase of $SrFeO_{2.86}$ (JCPDS card No. 039–0954) is identified in the samples containing high values of Sr (=0.3), which is in good agreement with that reported by others [47].

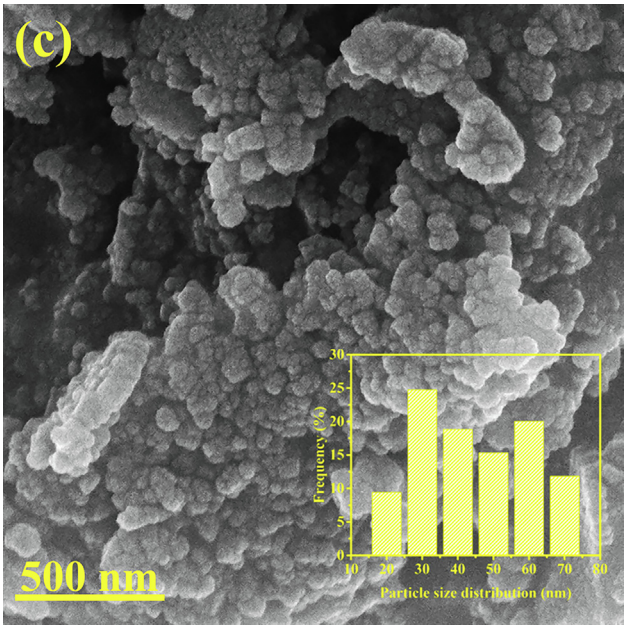

Fig. 5. (*continued*)

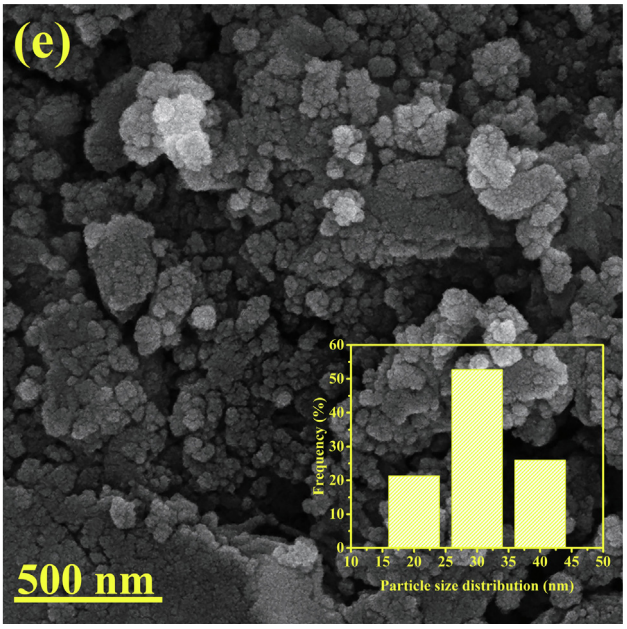

Fig. 5. (*continued*)

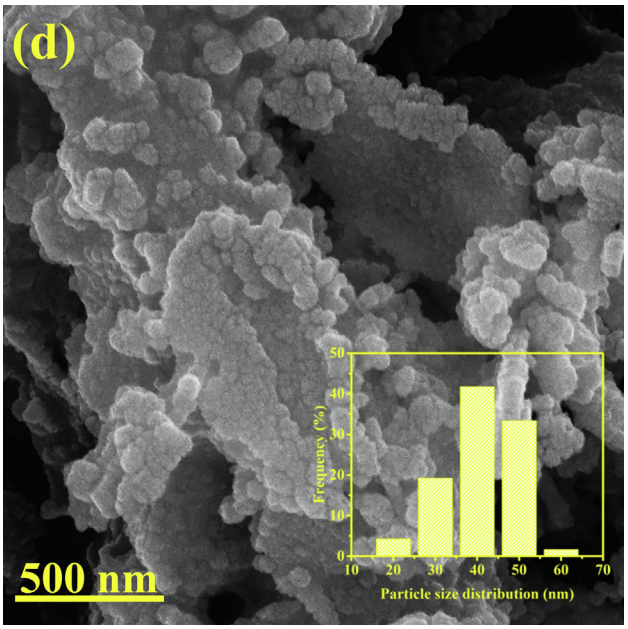

Fig. 5. (*continued*)

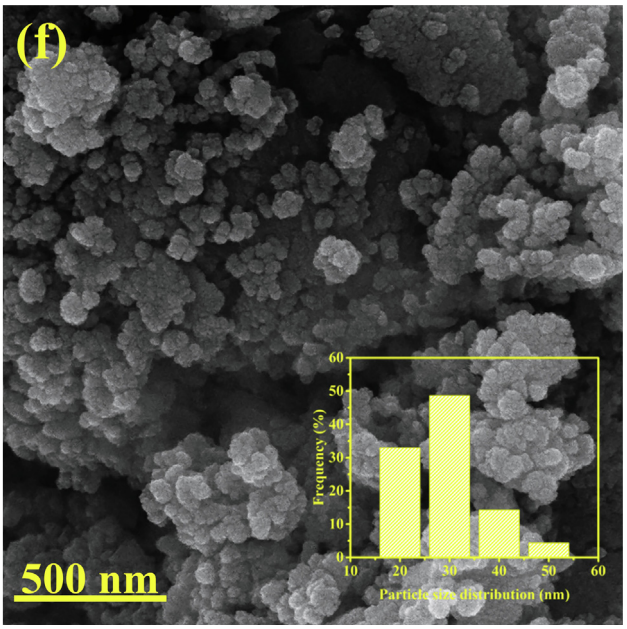

Fig. 5. (*continued*)

Also, to confirm the nanocrystalline nature of the prepared samples, the average of crystallite size was calculated by the refinement of the structural parameter by using the Rietveld method (Table 1). Also, Fig. 3 is presented to better understand how zinc and strontium ions influence the size of crystals. As seen in this figure, the average of crystallite size is drastically decreased by doping of Zn^{2+} and Sr^{2+} ions.

It is notable that the average of crystallite size can be depended upon to rates of nucleation and growth steps and doping by ions with different ionic radius can lead to a severe distortion in the lattice and consequently a decrease in rate of growth step as well as the average of crystallite size.

It is notable that Sr^{2+} (1.32 Å [19]) and Zn^{2+} (0.82 Å [36]) ions have larger sizes than Co^{2+} (0.75 Å [65]) and Fe^{3+} (0.64 Å [65]) ions. Therefore, some of these dopant ions tend to be at the grain boundaries, which can restrict grain growth by pinning the grain boundaries. On the other hand, this doping can also induce lattice strain. As a result, it can change not only the average of crystallite size but also lattice parameter. Furthermore, it can be expected that lattice strain increases by doping of Sr^{2+} and Zn^{2+} ions.

On the other hand, the lattice constant for the all synthesized samples was calculated by using the Rietveld method. The lattice constant of the all samples was presented in Table 1. Also, Fig. 4 illustrates the effect of doping of Sr^{2+} and Zn^{2+} ions on the lattice parameter. As seen, both divalent ions increase this structural parameter. However, it is well observed that the effect of zinc ions on the lattice parameter is much greater than that of strontium ions.

As mentioned, Sr^{2+} and Zn^{2+} ions have larger ionic radius compared with Co^{2+} and Fe^{3+} ions. Therefore, due to the formation of a large strain by doping these ions, secondary phases are more likely to form, which is in good agreement with that reported by others [47,66]. Increasing of lattice strain can be attributed to increase in dislocations, micro stresses, grain boundaries, coherency strains and crystallite

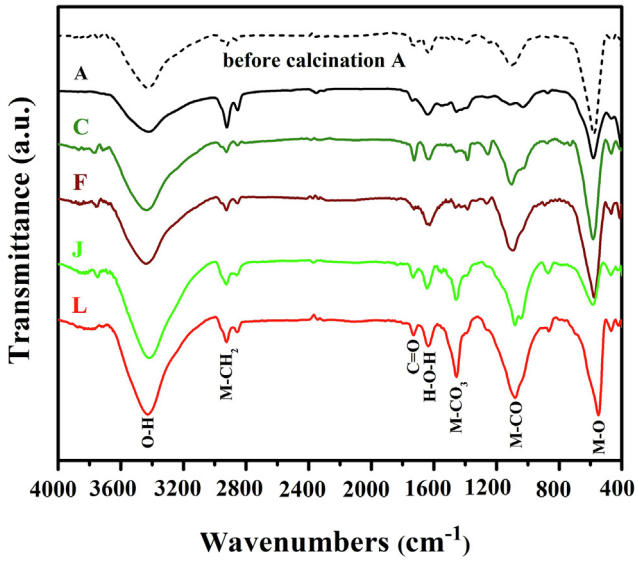

Fig. 6. FT-IR spectra for the selected samples.

Table 2
FTIR absorption frequency bands.

Sample code	Chemical composition	Tetrahedral (υ_1)	Octahedral (υ_2)
A	$CoFe_2O_4$	583	468
C	$Co_{0.89}Sr_{0.01}Zn_{0.1}Fe_2O_4$	583	469
F	$Co_{0.9}Sr_{0.05}Zn_{0.05}Fe_2O_4$	578	470
J	$Co_{0.6}Sr_{0.3}Zn_{0.1}Fe_2O_4$	588	470
L	$Sr_{0.3}Zn_{0.7}Fe_2O_4$	552	467

compactness. Consequently, unit cell volume of the synthesized samples is increased by doping of these two divalent ions (Table 1).

In addition, X-ray density (ρ_{th}) of the prepared samples was calculated from the values of the lattice parameter by using the following equation:

$$\rho_{th} = \frac{8.\ M}{N_a.\ a^3} \quad (1)$$

where a is the lattice parameter; N_a is the Avogadro's number; and M is the molecular weight of the synthesized ferrites. X-ray density of the prepared samples is listed in Table 1. As presented in Table 1, it is shown that the value of ρ_{th} changes with an increase in dopants concentration. This parameter is affected by the simultaneous the lattice parameter and the molecular weight of the synthesized ferrites. It is observed that X-ray density is increased by doping Sr^{2+} ions. The increase in X-ray density by doping Sr^{2+} ions is attributed to the increase in the molecular weight of the synthesized ferrites. It is notable that the ionic weights of Sr^{2+} (87.62 g/mol [67,68]) and Zn^{2+} (65.38 g/mol [69]) are higher than that of Co^{2+} (58.93 g/mol [70]) and Fe^{3+} (55.84 g/mol [69]). As observed, the ionic weights of Sr^{2+} ions is much higher than that of cobalt, so doping it can increase density regardless of its effect on the lattice parameter. However, the ionic weights of zinc and cobalt are close together, so the influence of doping by zinc on the density is determined simultaneously by the influence of the presence of this element on the lattice parameter and the ionic weight of the synthesized ferrite. Therefore, the variation of the structural parameters (Table 1) is non-monotonic with doped Zn concentration. Furthermore, it is observed that X-ray density of the synthesized ferrites is greater than bulk density, which can be attributed to the existence of the pores formed during ferrite synthesis and sintering of bulk samples. These results are in good agreement with that obtained by others [71].

3.3. FE-SEM analysis

Morphologies and particles size distribution of the samples A, B, C, F, J, and L are presented in Fig. 5. It is obvious that the morphology of the nanoparticles differs by doping Sr^{2+} and Zn^{2+} ions. In the all samples, it is observed that there is no particular morphology and the nanoparticles are highly agglomerated. It is accepted that the combustion process is known as a usual factor for the formation of agglomerated nanoparticles [2]. However, decrease in average size of the nanoparticles by doping Sr^{2+} and Zn^{2+} ions is well confirmed. Fig. 5(a) and (b) show that nanoparticles synthesized in the samples A and B have inhomogeneous shape and particles size distribution, which is in good agreement with that presented in the related article [1].

Fig. 5(c) shows a semi-spherical morphology for sample C with a noticeable decrease in the nanoparticles synthesized in this sample. Fig. 5(d) demonstrates the morphology of the sample F by a more

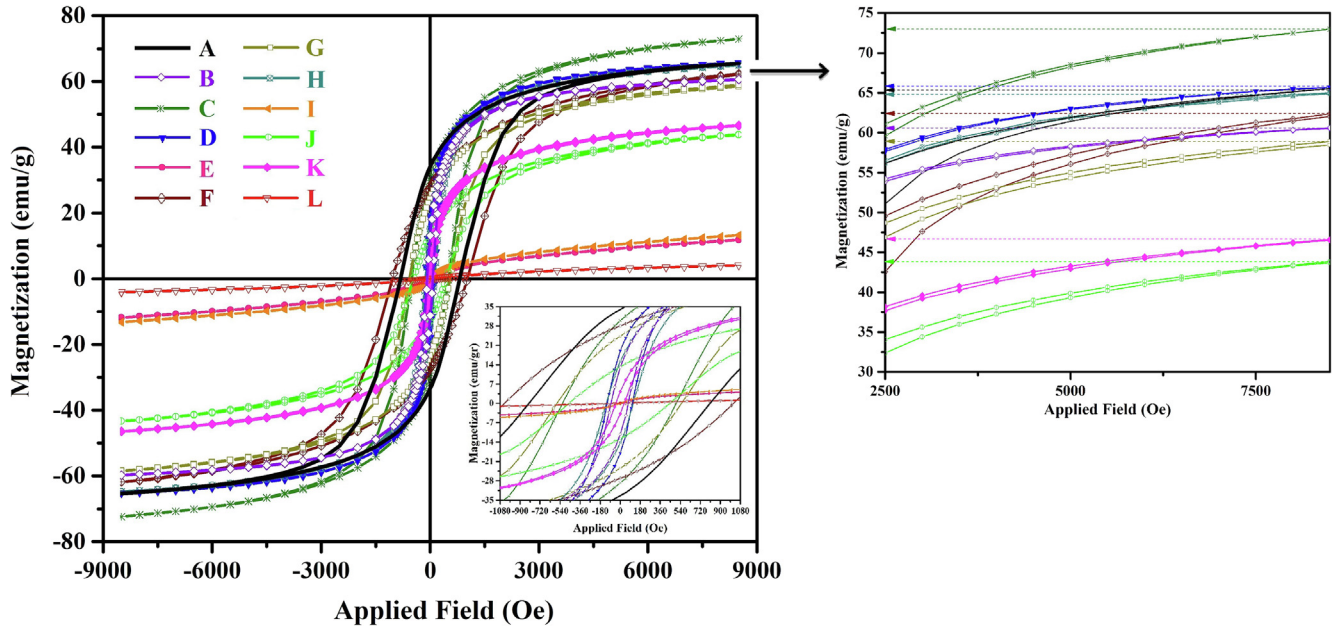

Fig. 7. M−H hysteresis loops of the synthesized samples at room temperature.

Table 3
Magnetic properties of Sr-Zn ferrite samples.

Sample code	Composition	M_s (emu/g)	M_r (emu/g)	H_c (Oe)	K × 10^3 (erg/g)	n_B	M_r/M_s
A	$CoFe_2O_4$	65.6	34	809.8	54.20	2.75	0.51
B	$Co_{0.5}Zn_{0.5}Fe_2O_4$	60.7	13	71.6	4.43	2.54	0.21
C	$Co_{0.89}Sr_{0.01}Zn_{0.1}Fe_2O_4$	72.9	29.8	503.4	37.44	3.06	0.40
D	$Co_{0.59}Sr_{0.01}Zn_{0.4}Fe_2O_4$	65.7	19.1	108.2	7.25	2.75	0.29
E	$Co_{0.29}Sr_{0.01}Zn_{0.7}Fe_2O_4$	12.1	0.04	7.2	0.08	0.51	0.00
F	$Co_{0.9}Sr_{0.05}Zn_{0.05}Fe_2O_4$	62.3	27.9	1019.2	64.79	2.61	0.44
G	$Co_{0.85}Sr_{0.05}Zn_{0.1}Fe_2O_4$	58.9	24.3	550.8	33.10	2.65	0.41
H	$Co_{0.55}Sr_{0.05}Zn_{0.4}Fe_2O_4$	64.9	15.3	118.2	7.82	2.72	0.23
I	$Co_{0.25}Sr_{0.05}Zn_{0.7}Fe_2O_4$	13.1	0.01	5.1	0.06	0.55	0.00
J	$Co_{0.6}Sr_{0.3}Zn_{0.1}Fe_2O_4$	43.8	13.2	444.9	19.88	1.83	0.30
K	$Co_{0.3}Sr_{0.3}Zn_{0.4}Fe_2O_4$	46.6	4.3	36.1	1.71	1.95	0.09
L	$Sr_{0.3}Zn_{0.7}Fe_2O_4$	4.4	0.01	23.4	0.10	0.18	0.00

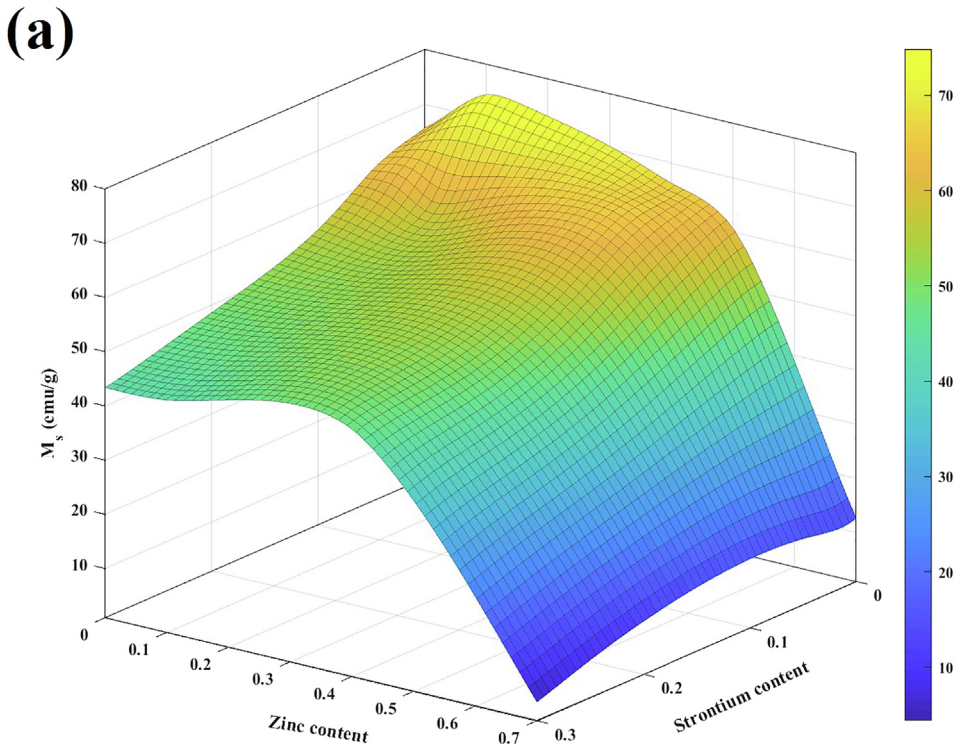

Fig. 8. Variation of magnetic properties as a function of Zn and Sr contents; (a) M_s, (b) M_r, and (c) H_c.

regular size distribution. These nanoparticles also have a semi-spherical shape that is highly agglomerated. As mentioned before, some of the dopant ions (i.e. Sr^{2+} and Zn^{2+} ions) can pin the grain boundaries and thus reduce the particle size. So, it can be expected that a more agglomerated structure is formed in the samples doped by these dopants. Furthermore, the magnetic nature of the synthesized nanoparticles and more surfaces to volume ratio in these nanoparticles in order to have lower surface energy can be effective on the morphology and agglomeration behavior. Fig. 5(e) is related to the morphology and particles size distribution of nanoparticles synthesized in the sample J, which shows a semi-spherical morphology, regular and well-distributed nanoparticles in comparison to previous ones that it can be attributed to more amount of Sr in the composition. Also, Fig. 5(f) demonstrates a well spherical shape for the sample L. Also, the average of nanoparticles size for the all samples was calculated by the microstructural image processing (MIP) software and is presented in Table 1. It can be seen that the crystallite size decreases from 77.1 (for the sample A) to 29.1 nm (for the sample L) with an increase in the amount of dopant ions. As seen, the general trend of these results is in agreement with those obtained by the Rietveld method. However, the averages of nanoparticles size measured by FE-SEM micrographs are larger than that of calculated by using XRD patterns (the Rietveld method). It should be noted that the Rietveld method measures the average of crystallite size, while the average of nanoparticles size can be obtained by FE-SEM micrographs and every nanoparticle can be formed by aggregation of the several crystallites/grains. Also, it is reported that strain over the surface of the nanoparticles leads to broadening of XRD peak profiles, which can affected average of particles size measured by using XRD patterns [9,72].

3.4. FT-IR spectroscopy

FT-IR spectra of the samples A, C, F, J, and L at room temperature in a wave number range of 400 to 4000 cm^{-1} are presented in Fig. 6. All FT-IR spectra in the described range demonstrate two well-defined peaks, first one around 467–470 cm^{-1} (υ_2) and the other near 552–588 cm^{-1} (υ_1), which are related to intrinsic stretching-vibrations of the oxygen bonds with metal cations in positions of the tetrahedral sites (A sites) and the octahedral sites (B sites). The weak frequency peak (υ_2) attributes to the intrinsic vibration of metal–oxygen bond at the B-sites and the high frequency peak (υ_1) shows the metal–oxygen vibration at the A-sites [45,73,74]. As seen, the normal mode of

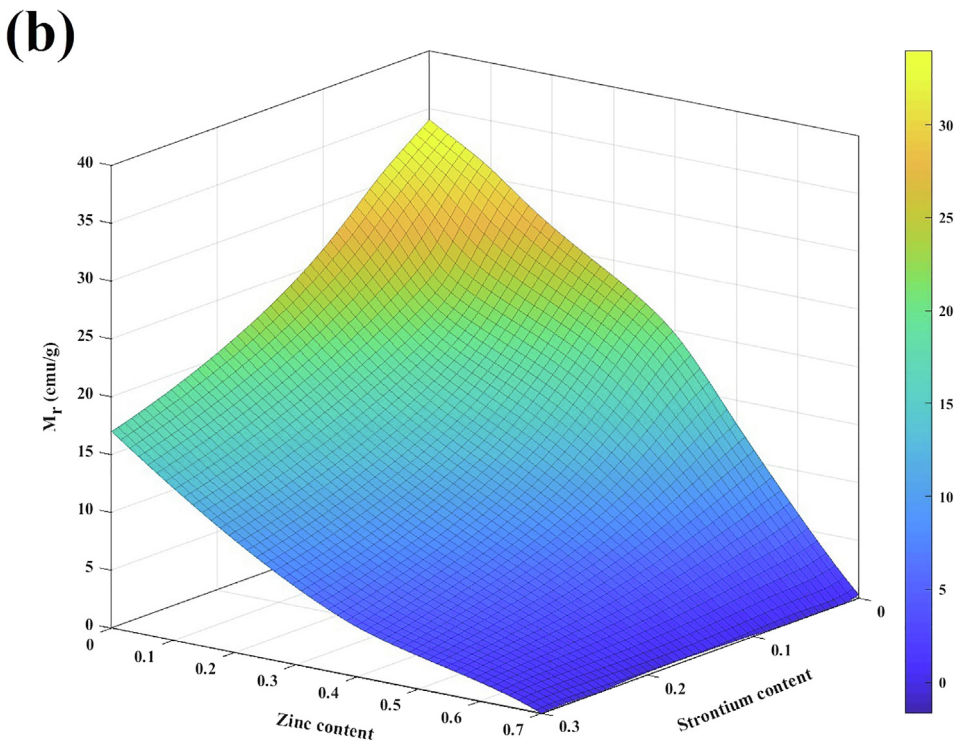

Fig. 8. (*continued*)

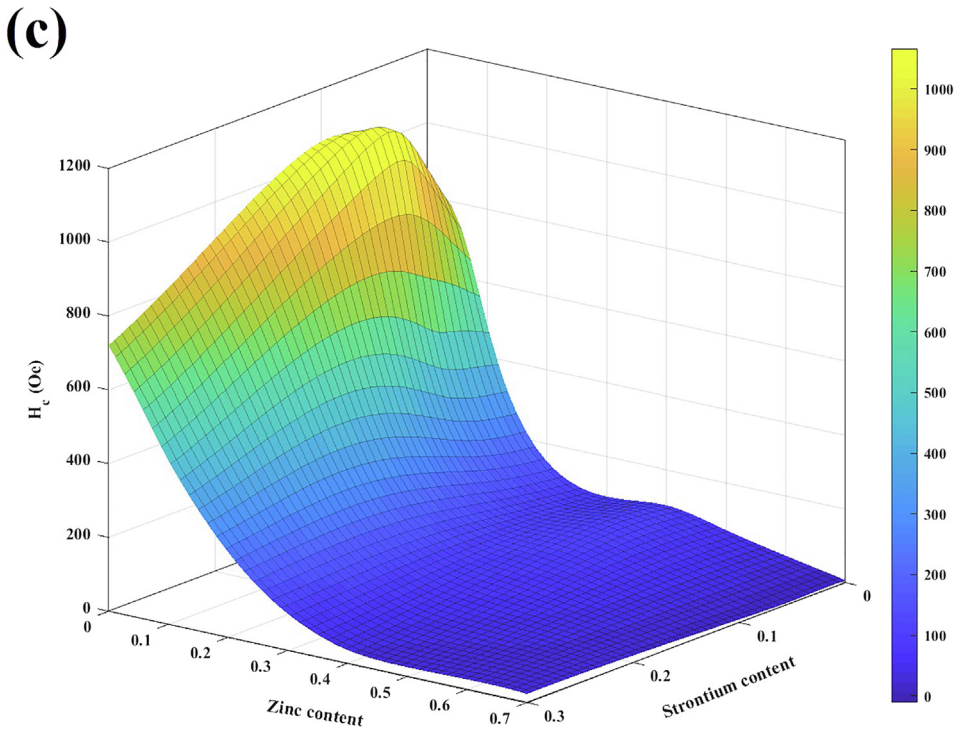

Fig. 8. (*continued*)

vibration of the A site is higher than that at B site, which can be due to the shorter bond length of tetrahedral than the octahedral. Accordingly, the presence of these two absorption bands confirms formation of the spinel structure [9,30,61]. The values of absorption frequency υ_1 and υ_2 are listed in Table 2. As seen, although all the doped samples have similar peaks compared to pure crystallites, but the substitution of Co^{2+} with Sr^{2+} and Zn^{2+} causes a slightly shift of the position of absorption bands. Minor shifting of peaks for the bands ν_1 and ν_2 with doping of Sr^{2+}- and Zn^{2+} ions can be due to vary distance between Fe^{3+}–O^{2-} in the octahedral and tetrahedral sites [37]. Also, the bands observed around 1080 and1450 cm^{-1} frequencies are related to the carboxylate anion [75,76]. The bands at 1730 cm^{-1} indicate C = O bond, which is very weak. Also, the bands around 2300 cm^{-1} represent the organic residues. The peaks appearing at 2850 and 2900 cm^{-1} are related to axial deformation of the C–H bond and C–H stretching vibration, respectively [61,77]. The other IR bands around 1630 and 3400 cm^{-1}

Table 4
A comparison between properties of $CoFe_2O_4$ magnetic nanoparticles synthesis of this study and other investigations.

Chemical composition	Crystallite size (nm)	M_s (emu/g)	H_c (Oe)	M_r (emu/g)	Synthesis route	Phase mode	Ref.
Sr^{2+} ion							
$Co_{1-x}Sr_xFe_2O_4$(x = 0.0, 0.01, 0.015, 0.02, 0.05, 0.1)	18–8	~38–56	~815–1500	~10.5–18	Sol-gel	Pure phase	[18]
$Co_{1-x}Sr_xFe_2O_4$(x = 0.0, 0.11, 0.42, 1.0)	53–62	38–63	1300–1740	18–25	Microwave-assisted combustion	Secondary phase (CoO, $SrCO_3$, $SrFeO_{2.96}$)	[47]
$Co_{0.4}Sr_{0.6}Fe_2O_4$	–	~36–54	~380–1800	~9–30	co-precipitation	Secondary phase ($SrCO_3$)	[66]
Zn^{2+} ion							
$Co_{1-x}Zn_xFe_2O_4$	7–10	14–49	1–22	0–0.87	co-precipitation	Pure phase	[45]
$Co_{1-x}Zn_xFe_2O_4$(x = 0.0, 0.2, 0.4, 0.6, 0.8, 1.0)	6–8	4–34	4–500	0.01–8.50	Microemulsion	Pure phase	[44]
$Co_{1-x}Zn_xFe_2O_4$(x = 0.0, 0.1, 0.2, 0.3, 0.4, 0.5, 0.6)	140–190	376–437	2–22	–	Sol-gel	Pure phase	[36]
$Co_{1-x}Zn_xFe_2O_4$(x = 0.0, 0.30, 0.46, 0.53)	5.9–6.7	109–157	3700–12000	–	surfactant-assisted thermaldecomposition	Pure phase	[89]
$Co_{1-x}Zn_xFe_2O_4$(x = 0.0, 0.03, 0.04, 0.05)	15–25	2–4	21–71	3–11	Sol-gel	Pure phase	[77]

appear due to the bending and stretching vibration of H_2O molecules [30,46]. However, by substitution of divalent ions Sr^{2+} and Zn^{2+} on cobalt site in cobalt ferrite, only minor changes are observed in spectrum.

3.5. VSM analysis

Typical magnetic hysteresis loops of the samples with the composition of $Co_{1-x-y}Sr_xZn_yFe_2O_4$ (where x = 0.0, 0.01, 0.05, 0.3 and y = 0.0, 0.05, 0.1, 0.4, 0.7) are shown in Fig. 7. Also, the magnetic moment (n_B in Bohr magneton) is computed by using the below formula [11,78]:

$$n_B = \frac{M_{\text{Spinel ferrite}} \times M_s}{5585} \tag{2}$$

where $M_{\text{Spinel ferrite}}$is molecular weight of the synthesized ferrite in g/mol and M_s is saturation magnetization in emu/g. On the other hand, values of the anisotropy constant (K) are calculated by using the following equation [78]:

$$K = \frac{H_c \times M_s}{0.98} \tag{3}$$

The magnetic characteristic parameters are presented in Table 3.

Hysteresis loop provides enough detail to obtain the required magnetic parameters and also to determine soft, hard or super-paramagnetic behavior of the investigated samples. It is well-known that the soft magnetic material has a narrow hysteresis loop with a low coercive force as well as a small remanence magnetization (M_r) [79]. While, the hard magnetic materials are known with a high coercive force and a high remanence value, so the magnetic field of the hard magnetic material can keep a long time [80]. As shown in Fig. 7 and Table 3, the magnetic properties of the synthesized samples are strongly influenced by doping of the zinc and strontium ions, so that some samples exhibit soft behavior (i.e. the samples E and I) and others show a hard/semi-hard behavior (i.e. the samples A, C, F, G, and J). As expected, the samples E and I have very low remanence ratio (M_r/M_s). It is well known that single-domain magnetic nanoparticles exhibit a super-paramagnetic behavior [81]. In this condition, magnetic nanoparticles display higher saturation magnetization and very low coercivity.

Fig. 8(a), (b) and (c) illustrate the variation of M_s, M_r and H_c versus dopants contents, respectively. As seen in Fig. 8(a), saturation magnetization decreases with doping of Sr^{2+}- and Zn^{2+}, so that this magnetic parameter decreases from 65.6 emu/g (in the sample A) to 4.4 emu/g (in the sample L) with an increase in dopants content, which can be attributed to the formation of the secondary phases. A similar trend is also observed for M_r (Fig. 8(b)). On the other hand, it is acceptable that magnetization of nanoparticles decreases with decreasing crystallite size due to the surface anisotropy energy of nano-scale ferrites [9,82–84]. As presented in Fig. 3, the average of crystallite size is drastically decreased by doping of Zn^{2+} and Sr^{2+} ions, which is in a good agreement with the trend of magnetization. Furthermore, changes in the cation distribution in the presence of Sr and Zn can affect the magnetic properties. For instance, researchers [44,46,85] reported that the Zn^{2+} ions seek to the tetrahedral sites of the ferrite sub lattice, thereby resulting in a decreased magnetic moment. On the other hand, Lima et al. [47] showed that the Sr^{2+} ions go mainly to octahedral sites. They revealed that the excess of the Sr^{2+} ions favors the production of paramagnetic phases. Therefore, when the strontium concentration is increased, the M_s and M_r decrease.

Fig. 8(c) shows that the maximum value of H_c is observed by the sample F with composition of $Co_{0.9}Sr_{0.05}Zn_{0.05}Fe_2O_4$ that it may be attributed to the pinning of the magnetic domains in the presence of small amounts of Sr^{2+} and Zn^{2+}. However, it is observed that H_c decreases with doping of higher value of Sr^{2+} and Zn^{2+}. This magnetic parameter is affected by various structural defects, i.e. dislocations, grain boundaries, anisotropy, and precipitates [86,87]. On the other

hand, in the single-domain region, the coercivity decreases with a decrease in the grain size because of thermal effects [88]. Therefore, smaller grain size in the presence of higher value of Sr^{2+} and Zn^{2+} can be attributed to a decrease in the coercivity.

The structural and magnetic properties of the nano-scale ferrites synthesized in the present study are compared with the obtained results in the previous works [19,36,44,45,47,66,77,89] in Table 4. As presented, it is shown that the nanoparticles doped by the simultaneous divalent dopants of Sr^{2+} and Zn^{2+} have better magnetic properties than that of obtained in most of the previous studies, so that the structural and magnetic properties of the nanoparticles synthesized in the presence study are enhanced by the simultaneous doping of these two dopants as compared to nanoparticles synthesized doped by only Zn^{2+} [43,90] or Sr^{2+} [19,47,66]. On the other hand, our magnetic investigations show that by simultaneous presence of these two dopants, a super-paramagnetic behavior can be observed and therefore these nanoparticles can have potential applications such as magnetic resonance imaging (MRI) contrast agents in ferrofluids based technology, information storage device, gas sensors and etc. [91].

4. Summery

In the present study, the magnetic nanoparticles of $Co_{1-x-y}Sr_xZn_yFe_2O_4$ (where x = 0.0, 0.01, 0.05, 0.3 and y = 0.0, 0.05, 0.1, 0.4, 0.7) were synthesized by using the sol–gel auto-combustion method. Based on DTA-TG results, the cubic spinel structure was formed during two different stages. Also, the obtained results showed that the cubic spinel structure of $CoFe_2O_4$ has been formed in the all samples. However, a secondary phase of $SrFeO_{2.86}$ was identified in the samples containing high values of Sr (=0.3). The average of crystallite size decreased in the presence of dopant elements of Zn and Sr, while the lattice parameter showed a completely opposite trend with the increase of these dopant elements. Also, it was confirmed that the morphology of the synthesized samples was affected by the presence of dopant elements of Zn and Sr, so that morphology of the nanoparticles changed to a semi-spherical morphology, regular and well-distributed nanoparticles by addition of values of dopants. Furthermore, it is revealed that the magnetic properties of cobalt ferrite nanoparticles were strongly dependent on the presence of these two dopants, so that these dopants changed the ferrimagnetic behavior of the cobalt ferrite nanoparticles to a superparamagnetic behavior.

Declaration of Competing Interest

The authors declare that they have no known competing financial interests or personal relationships that could have appeared to influence the work reported in this paper.

Appendix A. Supplementary data

Supplementary data to this article can be found online at https://doi.org/10.1016/j.jmmm.2020.166941.

References

[1] A.H. Ashour, A.I. El-Batal, M.I.A.A. Maksoud, G.S. El-Sayyad, S. Labib, E. Abdeltwab, M.M. El-Okr, Antimicrobial activity of metal-substituted cobalt ferrite nanoparticles synthesized by sol–gel technique, Particuology 40 (2018) 141–151.

[2] S.I. El-Dek, Effect of annealing temperature on the magnetic properties of CoFe 2O4 nanoparticles, Philos. Mag. Lett. 90 (2010) 233–240.

[3] M. Amiri, M. Salavati-Niasari, A. Akbari, Magnetic nanocarriers: Evolution of spinel ferrites for medical applications, Adv. Colloid Interface Sci. 265 (2019) 29–44.

[4] M.K.K. Satheeshkumar, E.R. Kumar, C. Srinivas, N. Suriyanarayanan, M. Deepty, C.L.L. Prajapat, T.V.C.V.C. Rao, D.L.L. Sastry, Study of structural, morphological and magnetic properties of Ag substituted cobalt ferrite nanoparticles prepared by honey assisted combustion method and evaluation of their antibacterial activity, J. Magn. Magn. Mater. 469 (2019) 691–697.

[5] A. Sathiya Priya, D. Geetha, N. Kavitha, Effect of Al substitution on the structural, electric and impedance behavior of cobalt ferrite, Vacuum 160 (2019) 453–460.

[6] R. Nongjai, S. Khan, K. Asokan, H. Ahmed, I. Khan, Magnetic and electrical properties of in doped cobalt ferrite nanoparticles, J. Appl. Phys. 112 (2012).

[7] K. Pubby, S.S. Meena, S.M. Yusuf, S. Bindra Narang, Cobalt substituted nickel ferrites via Pechini's sol–gel citrate route: X-band electromagnetic characterization, J. Magn. Magn. Mater. 466 (2018) 430–445.

[8] D. Lisjak, A. Mertelj, Anisotropic magnetic nanoparticles: A review of their properties, syntheses and potential applications, Prog. Mater Sci. 95 (2018) 286–328.

[9] M. Afshari, A. Rouhani Isfahani, S. Hasani, F. Davar, K. Jahanbani Ardakani, Effect of apple cider vinegar agent on the microstructure, phase evolution, and magnetic properties of CoFe 2 O 4 magnetic nanoparticles, Int. J. Appl. Ceram. Technol. 16 (2019) 1612–1621.

[10] M.S. Khandekar, N.L. Tarwal, I.S. Mulla, S.S. Suryavanshi, Nanocrystalline Ce doped CoFe2O4 as an acetone gas sensor, Ceram. Int. 40 (2014) 447–452.

[11] K.M. Srinivasamurthy, V.J. Angadi, S.P. Kubrin, S. Matteppanavar, D.A. Sarychev, P.M. Kumar, H.W. Azale, B. Rudraswamy, Tuning of ferrimagnetic nature and hyperfine interaction of Ni2+ doped cobalt ferrite nanoparticles for power transformer applications, Ceram. Int. 44 (2018) 9194–9203.

[12] M.I.A. Abdel Maksoud, G.S. El-Sayyad, A.H. Ashour, A.I. El-Batal, M.S. Abd-Elmonem, H.A.M. Hendawy, E.K. Abdel-Khalek, S. Labib, et al., Synthesis and characterization of metals-substituted cobalt ferrite [MxCo(1–x)Fe2O4; (M = Zn, Cu and Mn; x = 0 and 0.5)] nanoparticles as antimicrobial agents and sensors for Anagrelide determination in biological samples, Mater. Sci. Eng., C 92 (2018) 644–656.

[13] J. Venturini, R.Y.S. Zampiva, S. Arcaro, C.P. Bergmann, Sol-gel synthesis of substoichiometric cobalt ferrite (CoFe2O4) spinels: Influence of additives on their stoichiometry and magnetic properties, Ceram. Int. 44 (2018) 12381–12388.

[14] J. Feng, R. Xiong, Y. Liu, F. Su, X. Zhang, Preparation of cobalt substituted zinc ferrite nanopowders via auto- combustion route : an investigation to their structural and magnetic properties, J. Mater. Sci.: Mater. Electron. (2018).

[15] H.R. Noormohamadi, M.R. Fat'hi, M. Ghaedi, Fabrication of polyethyleneimine modified cobalt ferrite as a new magnetic sorbent for the micro-solid phase extraction of tartrazine from food and water samples, J. Colloid Interface Sci. 531 (2018) 343–351.

[16] Pervaiz, E., Gul, I.H., "Structural, Electrical and Magnetic Studies of Gd Nanoparticles doped Cobalt Ferrite", International Journal of Current Engineering and Technology, pp. 377–387, 2012.

[17] M. Gharibshahian, M.S. Nourbakhsh, O. Mirzaee, Evaluation of the superparamagnetic and biological properties of microwave assisted synthesized Zn & Cd doped CoFe2O4 nanoparticles via Pechini sol–gel method, J. Sol-Gel Sci. Technol. 85 (2018) 684–692.

[18] A. Ghasemi, Compositional dependence of magnetization reversal mechanism, magnetic interaction and Curie temperature of Co1-xSrxFe2O4 spinel thin film, J. Alloy. Compd. 645 (2015) 467–477.

[19] R. Kumar, M. Kar, Lattice strain induced magnetism in substituted nanocrystalline cobalt ferrite, J. Magn. Magn. Mater. 416 (2016) 335–341.

[20] R.S. Yadav, I. Kuřitka, J. Vilcakova, J. Havlica, L. Kalina, P. Urbánek, M. Machovsky, D. Skoda, et al., Sonochemical synthesis of Gd3+doped CoFe2O4spinel ferrite nanoparticles and its physical properties, Ultrason. Sonochem. 40 (2018) 773–783.

[21] G. Wang, Y. Ma, Z. Wei, M. Qi, Development of multifunctional cobalt ferrite/graphene oxide nanocomposites for magnetic resonance imaging and controlled drug delivery, Chem. Eng. J. 289 (2016) 150–160.

[22] S.M. Ansari, B.B. Sinha, K.R. Pai, S.K. Bhat, Y.R. Ma, D. Sen, Y.D. Kolekar, C.V. Ramana, Controlled surface/interface structure and spin enabled superior properties and biocompatibility of cobalt ferrite nanoparticles, Appl. Surf. Sci. 459 (2018) 788–801.

[23] J.C. Fariñas, R. Moreno, A. Pérez, M.A. García, M. García-Hernández, M.D. Salvador, A. Borrell, Microwave-assisted solution synthesis, microwave sintering and magnetic properties of cobalt ferrite, J. Eur. Ceram. Soc. 38 (2018) 2360–2368.

[24] A. Hassani, P. Eghbali, Ö. Metin, Sonocatalytic removal of methylene blue from water solution by cobalt ferrite/mesoporous graphitic carbon nitride (CoFe2O4/mpg-C3N4) nanocomposites: response surface methodology approach, Environ. Sci. Pollut. Res. (2018).

[25] L.T. Lu, N.T. Dung, L.D. Tung, C.T. Thanh, O.K. Quy, N.V. Chuc, S. Maenosono, N.T.K. Thanh, Synthesis of magnetic cobalt ferrite nanoparticles with controlled morphology, monodispersity and composition: The influence of solvent, surfactant, reductant and synthetic conditions, Nanoscale 7 (2015) 19596–19610.

[26] E. Ferdosi, H. Bahiraei, D. Ghanbari, Investigation the photocatalytic activity of CoFe2O4/ZnO and CoFe2O4/ZnO/Ag nanocomposites for purification of dye pollutants, Sep. Purif. Technol. 211 (2019) 35–39.

[27] Nasrin, S., Chowdhury, F.-U.-Z., Hasan, M.M., Hossen, M.M., Ullah, S.M., Hoque, S. M., "Effect of zinc substitution on structural, morphological and magnetic properties of cobalt nanocrystalline ferrites prepared by co-precipitation method", Journal of Materials Science: Materials in Electronics, 2018.

[28] S. Zare, A.A. Ati, S. Dabagh, R.M. Rosnan, Z. Othaman, Synthesis, structural and magnetic behavior studies of Zn-Al substituted cobalt ferrite nanoparticles, J. Mol. Struct. 1089 (2015) 25–31.

[29] G.B.M. Melo, M.L.N. Grillo, R.S. de Biasi, Synthesis and magnetic properties of CoAlFe2O4 nanoparticles, Ceram. Int. 8 (2018) 288–294.

[30] H.S. Mund, B.L. Ahuja, Structural and magnetic properties of Mg doped cobalt ferrite nano particles prepared by sol-gel method, Mater. Res. Bull. 85 (2017) 228–233.

[31] L. Ai, J. Jiang, Influence of annealing temperature on the formation, microstructure

and magnetic properties of spinel nanocrystalline cobalt ferrites, Curr. Appl Phys. 10 (2010) 284–288.
[32] T. Dippong, E.A. Levei, C. Tanaselia, M. Gabor, M. Nasui, L. Barbu Tudoran, G. Borodi, Magnetic properties evolution of the CoxFe3-xO4/SiO2 system due to advanced thermal treatment at 700˚C and 1000˚C, J. Magn. Magn. Mater. 410 (2016) 47–54.
[33] M. Ştefănescu, T. Dippong, M. Stoia, O. Ştefănescu, Study on the obtaining of cobalt oxides by thermal decomposition of some complex combinations, undispersed and dispersed in SiO2 matrix, J. Therm. Anal. Calorim. 94 (2008) 389–393.
[34] R.V. Kumar, A.V. Anupama, R. Kumar, H.K. Choudhary, V.B. Khopkar, G. Aravind, B. Sahoo, Cation distributions and magnetism of Al-substituted CoFe2O4 – NiFe2O4 solid solutions synthesized by sol-gel auto-combustion method, Ceram. Int. 44 (2018) 20708–20715.
[35] K.P. Chae, W.K. Kim, J.G. Lee, Y.B. Lee, Magnetic Properties of Ti-Doped Ultrafine CoFe2O4 Powder Grown by the Sol Gel Method, Hyperfine Interact. 136–137 (2001) 65–72.
[36] M. Atif, M.W. Asghar, M. Nadeem, W. Khalid, Z. Ali, S. Badshah, Synthesis and investigation of structural, magnetic and dielectric properties of zinc substituted cobalt ferrites, J. Phys. Chem. Solids 123 (2018) 36–42.
[37] A.P. Amaliya, S. Anand, S. Pauline, Investigation on structural, electrical and magnetic properties of titanium substituted cobalt ferrite nanocrystallites, J. Magn. Magn. Mater. 467 (2018) 14–28.
[38] C.C. Naik, S.K. Gaonkar, I. Furtado, A.V. Salker, Effect of Cu2+ substitution on structural, magnetic and dielectric properties of cobalt ferrite with its enhanced antimicrobial property, J. Mater. Sci.: Mater. Electron. 29 (2018) 14746–14761.
[39] Z.K. Heiba, M.B. Mohamed, S.I. Ahmed, Cation distribution correlated with magnetic properties of cobalt ferrite nanoparticles defective by vanadium doping, J. Magn. Magn. Mater. 441 (2017) 409–416.
[40] H. Nikmanesh, M. Eshraghi, S. Karimi, Cation distribution, magnetic and structural properties of CoCrxFe2-xO4: Effect of calcination temperature and chromium substitution, J. Magn. Magn. Mater. 471 (2019) 294–303.
[41] E.O. Huber, C.H. Bastiaenen, H.A. Bischoff-Ferrari, A. Meichtry, R.A. De Bie, Development of the knee osteoarthritis patient education questionnaire: A new measure for evaluating preoperative patient education programmes for patients undergoing total knee replacement, Swiss Medical Weekly 145 (2015) 377–387.
[42] K.K. Patankar, D.M. Ghone, V.L. Mathe, S.D. Kaushik, Structural and physical property study of sol–gel synthesized CoFe2−xHoxO4nano ferrites, J. Magn. Magn. Mater. 454 (2018) 71–77.
[43] T. Dippong, F. Goga, E.A. Levei, O. Cadar, Influence of zinc substitution with cobalt on thermal behaviour, structure and morphology of zinc ferrite embedded in silica matrix, J. Solid State Chem. 275 (2019) 159–166.
[44] C. Singh, S. Jauhar, V. Kumar, J. Singh, S. Singhal, Synthesis of zinc substituted cobalt ferrites via reverse micelle technique involving in situ template formation: A study on their structural, magnetic, optical and catalytic properties, Mater. Chem. Phys. 156 (2015) 188–197.
[45] I. Sharifi, H. Shokrollahi, Nanostructural, magnetic and Mössbauer studies of nanosized Co1-xZnxFe2O4synthesized by co-precipitation, J. Magn. Magn. Mater. 324 (2012) 2397–2403.
[46] D.M. Jnaneshwara, D.N. Avadhani, B. Daruka Prasad, B.M. Nagabhushana, H. Nagabhushana, S.C. Sharma, S.C. Prashantha, C. Shivakumara, Effect of zinc substitution on the nanocobalt ferrite powders for nanoelectronic devices, J. Alloy. Compd. 587 (2014) 50–58.
[47] A.C. Lima, A.P.S. Peres, J.H. Araújo, M.A. Morales, S.N. Medeiros, J.M. Soares, D.M.A. Melo, A.S. Carriço, The effect of Sr2+ on the structure and magnetic properties of nanocrystalline cobalt ferrite, Mater. Lett. 145 (2015) 56–58.
[48] S. Hasani, M. Panjepour, M. Shamanian, A study of the effect of aluminum on MoSi2 formation by self-propagation high-temperature synthesis, J. Alloy. Compd. 502 (2010).
[49] S. Hasani, M. Panjepour, M. Shamanian, Effect of atmosphere and heating rate on mechanism of MoSi < inf > 2 < /inf > formation during self-propagating high-temperature synthesis, J. Therm. Anal. Calorim. 107 (2012).
[50] X. Wu, H. Yu, H. Dong, Enhanced infrared radiation properties of CoFe2O4 by doping with Y3+ via sol–gel auto-combustion, Ceram. Int. 40 (2014) 12883–12889.
[51] M. Amiri, M. Salavati-Niasari, A. Akbari, R. Razavi, Sol–gel auto-combustion synthesize and characterization of a novel anticorrosive cobalt ferrite nanoparticles dispersed in silica matrix, J. Mater. Sci.: Mater. Electron. 28 (2017) 10495–10508.
[52] S.H. Xiao, W.F. Jiang, L.Y. Li, X.J. Li, Low-temperature auto-combustion synthesis and magnetic properties of cobalt ferrite nanopowder, Mater. Chem. Phys. 106 (2007) 82–87.
[53] M.A. Gabal, A.A. Al-Juaid, S. El-Rashed, M.A. Hussein, Synthesis and characterization of nano-sized CoFe 2 O 4 via facile methods: A comparative study, Mater. Res. Bull. 89 (2017) 68–78.
[54] M. Shan, S. Ding, J. Hua, W. Cui, J.J. Wang, J.J. Wang, Effect of annealing temperature on structure and magnetic properties of sol-gel synthesized Co0.8Fe2.2O4/SiO2 nanocomposites, J. Sol-Gel Sci. Technol. 88 (2018) 593–600.
[55] F. Falsafi, B. Hashemi, A. Mirzaei, E. Fazio, F. Neri, N. Donato, S.G. Leonardi, G. Neri, Sm-doped cobalt ferrite nanoparticles: A novel sensing material for conductometric hydrogen leak sensor, Ceram. Int. 43 (2017) 1029–1037.
[56] A.R. Rouhani, A.H. Esmaeil-Khanian, F. Davar, S. Hasani, The effect of agarose content on the morphology, phase evolution, and magnetic properties of CoFe 2 O 4 nanoparticles prepared by sol-gel autocombustion method, Int. J. Appl. Ceram. Technol. 15 (2018) 758–765.
[57] I. Barin, Thermochemical Data of Pure Substances, Wiley, Weinheim, 1995.
[58] A. Shanmugavani, R. Kalai Selvan, S. Layek, C. Sanjeeviraja, Size dependent electrical and magnetic properties of ZnFe2O4 nanoparticles synthesized by the combustion method: Comparison between aspartic acid and glycine as fuels, J. Magn. Magn. Mater. 354 (2014) 363–371.
[59] S.K. Rakshit, S.C. Parida, S. Dash, Z. Singh, B.K. Sen, V. Venugopal, Thermodynamic studies on SrFe12O19(s), SrFe2O4(s), Sr2Fe2O5(s) and Sr3Fe2O6(s), J. Solid State Chem. 180 (2007) 523–532.
[60] E.R. Schmidt, F.H.S. Vermaas, Differential thermal analysis and cell dimensions of some natural magnetites, Am. Mineral. 40 (1955) 422–431.
[61] S.M. Hashemi, S. Hasani, K. Jahanbani Ardakani, F. Davar, The effect of simultaneous addition of ethylene glycol and agarose on the structural and magnetic properties of CoFe2O4 nanoparticles prepared by the sol-gel auto-combustion method, J. Magn. Magn. Mater. 492 (2019) 165714.
[62] B. Pourgolmohammad, S.M. Masoudpanah, M.R. Aboutalebi, Synthesis of CoFe 2 O 4 powders with high surface area by solution combustion method: Effect of fuel content and cobalt precursor, Ceram. Int. 43 (2017) 3797–3803.
[63] P. Laokul, S. Arthan, S. Maensiri, E. Swatsitang, Magnetic and Optical Properties of CoFe2O4 Nanoparticles Synthesized by Reverse Micelle Microemulsion Method, J. Supercond. Novel Magn. 28 (2015) 2483–2489.
[64] P. Vlazan, M. Stoia, Structural and magnetic properties of CoFe2O4 nanopowders, prepared using a modified Pechini method, Ceram. Int. 44 (2018) 530–536.
[65] L. Kumar, P. Kumar, M. Kar, Cation distribution by Rietveld technique and magnetocrystalline anisotropy of Zn substituted nanocrystalline cobalt ferrite, J. Alloy. Compd. 551 (2013) 72–81.
[66] E.H. El-Ghazzawy, Effect of heat treatment on structural, magnetic, elastic and optical properties of the co-precipitated Co0.4Sr0.6Fe2O4, J. Magn. Magn. Mater. 497 (2020).
[67] N.A. Bezhin, I.I. Dovhyi, A.Y. Lyapunov, Sorption of strontium by sorbents on the base of di-(tert-butylcyclohexano)-18-crown-6 with use of various diluents, J. Radioanal. Nucl. Chem. 311 (2017) 317–322.
[68] K. Kirdsiri, R. Raja Ramakrishna, B. Damdee, H.J. Kim, S. Kaewjaeng, S. Kothan, J. Kaewkhao, Investigations of optical and luminescence features of Sm3+ doped Li2O-MO-B2O3 (M =Mg/Ca/Sr/Ba) glasses mixed with different modifier oxides as an orange light emitting phosphor for WLED's, J. Alloy. Compd. 749 (2018) 197–204.
[69] B. Daruka Prasad, H. Nagabhushana, K. Thyagarajan, B.M. Nagabhushana, D.M. Jnaneshwara, S.C. Sharma, C. Shivakumara, N.O. Gopal, et al., Temperature dependent magnetic ordering and electrical transport behavior of nano zinc ferrite from 20 to 800K, J. Alloy. Compd. 590 (2014) 184–192.
[70] D.D. Dung, N.B. Doan, N.Q. Dung, L.H. Bac, N.H. Linh, L.T.H. Thanh, D.V. Thiet, N.N. Trung, et al., Role of Co dopants on the structural, optical and magnetic properties of lead-free ferroelectric Na0.5Bi0.5TiO3 materials, J. Sci.: Adv. Mater. Devices 4 (2019) 584–590.
[71] M.K. Kokare, N.A. Jadhav, Y. Kumar, K.M. Jadhav, S.M. Rathod, Effect of Nd3+doping on structural and magnetic properties of Ni0.5Co0.5Fe2O4 nanocrystalline ferrites synthesized by sol-gel auto combustion method, J. Alloy. Compd. 748 (2018) 1053–1061.
[72] M.M. El-Okr, M.A. Salem, M.S. Salim, R.M. El-Okr, M. Ashoush, H.M. Talaat, Synthesis of cobalt ferrite nano-particles and their magnetic characterization, J. Magn. Magn. Mater. 323 (2011) 920–926.
[73] M. Ben Ali, K. El Maalam, H. El Moussaoui, O. Mounkachi, M. Hamedoun, R. Masrour, E.K. Hlil, A. Benyoussef, Effect of zinc concentration on the structural and magnetic properties of mixed Co-Zn ferrites nanoparticles synthesized by sol/gel method, J. Magn. Magn. Mater. 398 (2016) 20–25.
[74] A.M. Shaikh, S.A. Jadhav, S.C. Watawe, B.K. Chougule, Infrared spectral studies of Zn-substituted Li–Mg ferrites, Mater. Lett. 44 (2000) 192–196.
[75] G. Mustafa, M.U. Islam, W. Zhang, M.I. Arshad, Y. Jamil, H. Anwar, G. Murtaza, M. Hussain, et al., Investigation of the Role of Ce3+ Substituted Ions on Dielectric Properties of Co-Cr Ferrites Prepared by Co-precipitation Method, J. Electron. Mater. 45 (2016) 5830–5838.
[76] V.P. Senthil, J. Gajendiran, S.G. Raj, T. Shanmugavel, G. Ramesh Kumar, C. Parthasaradhi Reddy, Study of structural and magnetic properties of cobalt ferrite (CoFe2O4) nanostructures, Chem. Phys. Lett. 695 (2018) 19–23.
[77] V.K. Lakshmi, G.S. Kumar, A. Anugraha, T. Raguram, K.S. Rajni, Structural and Magnetic Studies of Zinc Substituted Cobalt Ferrite Nanoparticles prepared by Sol-Gel Technique, IOP Conf. Series: Mater. Sci. Eng. 577 (2019) 012068.
[78] T.R. Tatarchuk, N.D. Paliychuk, M. Bououdina, B. Al-Najar, M. Pacia, W. Macyk, A. Shyichuk, Effect of cobalt substitution on structural, elastic, magnetic and optical properties of zinc ferrite nanoparticles, J. Alloy. Compd. 731 (2018) 1256–1266.
[79] B. Fischer, J. Wagner, M. Schmitt, R. Hempelmann, Tuning the relaxation behaviour by changing the content of cobalt in CoxFe3−xO4 ferrofluids, J. Phys.: Condens. Matter 17 (2005) 7875–7883.
[80] C. Chi, J.-W. Lv, D. Wang, Calibration of triaxial magnetometer with ellipsoid fitting method, IOP Conf. Ser.: Earth Environ. Sci. 37 (2019) 032015.
[81] Q. Song, Z.J. Zhang, Correlation between Spin−Orbital Coupling and the Superparamagnetic Properties in Magnetite and Cobalt Ferrite Spinel Nanocrystals, J. Phys. Chem. B 110 (2006) 11205–11209.
[82] X. Cao, H. Dong, Y. Tan, J. Meng, Investigation of Synthesis and Magnetic Properties of Rod-Shaped CoFe2O4 via Precipitation-Topotactic Reaction Employing α-FeOOH and γ-FeOOH As Templates, J. Electron. Mater. 47 (2018) 2920–2928.
[83] B. Aslibeiki, Magnetic interactions and hysteresis loops study of Co/CoFe2O4 nanoparticles, Ceram. Int. 42 (2016) 6413–6421.
[84] R. Zhang, L. Sun, Z. Wang, W. Hao, E. Cao, Y. Zhang, Dielectric and magnetic properties of CoFe2O4 prepared by sol-gel auto-combustion method, Mater. Res. Bull. 98 (2018) 133–138.
[85] G. Vaidyanathan, S. Sendhilnathan, R. Arulmurugan, Structural and magnetic properties of Co1−xZnxFe2O4 nanoparticles by co-precipitation method, J. Magn.

Magn. Mater. 313 (2007) 293–299.
[86] S. Hasani, M. Shamanian, A. Shafyei, P. Behjati, M. Nezakat, M. Fathi-Moghaddam, J.A. Szpunar, Influence of annealing treatment on micro/macro-texture and texture dependent magnetic properties in cold rolled FeCo-7.15V alloy, J. Magn. Magn. Mater. 378 (2015).
[87] Hasani, S., Shamaniana, M., Shafyeia, A., Behjati, P., Szpunar, J.A., Fathi-Moghaddam, M., "Nano/sub-micron crystallization of Fe-Co-7.15V alloy by thermo-mechanical process to improve magnetic properties", Materials Science and Engineering B: Solid-State Materials for Advanced Technology, Vol. 190, 2014.
[88] J.N. Dahal, L. Wang, S.R. Mishra, V.V. Nguyen, J.P. Liu, Synthesis and magnetic properties of SrFe12 − x − yAlxCoyO19 nanocomposites prepared via autocombustion technique, J. Alloy. Compd. 595 (2014) 213–220.
[89] V. Mameli, A. Musinu, A. Ardu, G. Ennas, D. Peddis, D. Niznansky, C. Sangregorio, C. Innocenti, et al., Studying the effect of Zn-substitution on the magnetic and hyperthermic properties of cobalt ferrite nanoparticles, Nanoscale 8 (2016) 10124–10137.
[90] S. Singhal, T. Namgyal, S. Bansal, K. Chandra, Effect of Zn Substitution on the Magnetic Properties of Cobalt Ferrite Nano Particles Prepared Via Sol-Gel Route, J. Electromagn. Anal. Appl. 02 (2010) 376–381.
[91] E. Ranjith Kumar, R. Jayaprakash, G. Sarala Devi, P. Siva Prasada Reddy, Synthesis of Mn substituted CuFe2O4 nanoparticles for liquefied petroleum gas sensor applications, Sens. Actuators, B 191 (2014) 186–191.